Engineering xxx (xxxx) xxx

Contents lists available at ScienceDirect

Engineering

journal homepage: www.elsevier.com/locate/eng

Research
Medical Engineering—Article

Ionically Imprinting-Based Copper (Ⅱ) Label-Free Detection for Preventing Hearing Loss

Huan Wang [a,c,#,*], Hui Zhang [b,#], Xiaoli Zhang [d], Hong Chen [d], Ling Lu [d,*], Renjie Chai [b,e,f,g,h,*]

[a] The Eighth Affiliated Hospital, Sun Yat-Sen University, Shenzhen 518033, China
[b] State Key Laboratory of Digital Medical Engineering, Department of Otolaryngology Head and Neck Surgery, Zhongda Hospital & Advanced Institute for Life and Health, Southeast University, Nanjing 210096, China
[c] Guangdong Key Laboratory for Biomedical Measurements and Ultrasound Imaging, Department of Biomedical Engineering, Shenzhen University, Shenzhen 518060, China
[d] Department of Otolaryngology Head and Neck Surgery, Jiangsu Provincial Key Medical Discipline, Nanjing Drum Tower Hospital, The Affiliated Hospital of Nanjing University Medical School, Nanjing 210008, China
[e] Co-Innovation Center of Neuroregeneration, Nantong University, Nantong 226001, China
[f] Department of Otolaryngology Head and Neck Surgery, Sichuan Provincial People's Hospital, University of Electronic Science and Technology of China, Chengdu 610072, China
[g] Institute for Stem Cell and Regeneration, Chinese Academy of Science, Beijing 100101, China
[h] Beijing Key Laboratory of Neural Regeneration and Repair, Capital Medical University, Beijing 100069, China

ARTICLE INFO

Article history:
Received 15 July 2023
Revised 21 August 2023
Accepted 3 September 2023
Available online 15 September 2023

Keywords:
Structural color
Microfluidics
Ionic imprinting
Label-free detection
Hearing loss

ABSTRACT

Copper is a microelement with important physiological functions in the body. However, the excess copper ion (Cu^{2+}) may cause severe health problems, such as hair cell apoptosis and the resultant hearing loss. Therefore, the assay of Cu^{2+} is important. We integrate ionic imprinting technology (IIT) and structurally colored hydrogel beads to prepare chitosan-based ionically imprinted hydrogel beads (IIHBs) as a low-cost and high-specificity platform for Cu^{2+} detection. The IIHBs have a macroporous microstructure, uniform size, vivid structural color, and magnetic responsiveness. When incubated in solution, IIHBs recognize Cu^{2+} and exhibit a reflective peak change, thereby achieving label-free detection. In addition, benefiting from the IIT, the IIHBs display good specificity and selectivity and have an imprinting factor of 19.14 at 100 $\mu mol \cdot L^{-1}$. These features indicated that the developed IIHBs are promising candidates for Cu^{2+} detection, particularly for the prevention of hearing loss.

© 2023 THE AUTHORS. Published by Elsevier LTD on behalf of Chinese Academy of Engineering and Higher Education Press Limited Company. This is an open access article under the CC BY-NC-ND license (http://creativecommons.org/licenses/by-nc-nd/4.0/).

1. Introduction

Hearing loss is a serious and widespread disease affecting more than 1.5 billion people worldwide, more than 400 million of whom have moderate or severe hearing loss [1]. This disease not only reduces the quality of life but also increases the psychological burden on patients; therefore, it is crucial to prevent and treat hearing loss [2–5]. Among the various treatments, a feasible strategy is to reduce the intake of heavy metal ions, such as lead, cadmium, and copper. Copper agents are widely used in agriculture and industry [6–10]. Although copper is an important microelement in the human body, the excess uptake of copper ions (Cu^{2+}) in the environment and foods often causes severe health problems [11–13]. Excess Cu^{2+} generates hydroxyl radicals and induces apoptosis in hair cells (HCs), resulting in hearing loss [14–18]. Therefore, it is necessary to control Cu^{2+} uptake. Monitoring Cu^{2+} levels in foods and drinking water is a possible method. Many technologies, including fluorescence [19–21], spectrophotometry [22], inductively coupled plasma-atomic emission spectrometry [23], inductively coupled plasma mass spectrometry [24], atomic absorption spectroscopy [25], and electrochemistry [26,27]. Despite their high accuracy and specificity, these techniques are limited by the complex pretreatment of samples and expensive equipment. Therefore, a novel facile, low-cost, and high-specificity platform for Cu^{2+} detection is still lacking.

We developed chitosan (CS)-based Cu^{2+} ionic imprinted hydrogel bead (IIHB) with an inverse opal structure for the label-free detection of Cu^{2+} (Fig. 1). CS is a natural-derived polymer with abundant functional groups that can form coordination bonds

* Corresponding authors.
E-mail addresses: wangh679@mail.sysu.edu.cn (H. Wang), entluling60@126.com (L. Lu), renjiec@seu.edu.cn (R. Chai).
# These authors contributed equally to this work.

https://doi.org/10.1016/j.eng.2023.09.001
2095-8099/© 2023 THE AUTHORS. Published by Elsevier LTD on behalf of Chinese Academy of Engineering and Higher Education Press Limited Company.
This is an open access article under the CC BY-NC-ND license (http://creativecommons.org/licenses/by-nc-nd/4.0/).

Please cite this article as: H. Wang, H. Zhang, X. Zhang et al., Ionically Imprinting-Based Copper (Ⅱ) Label-Free Detection for Preventing Hearing Loss, Engineering, https://doi.org/10.1016/j.eng.2023.09.001

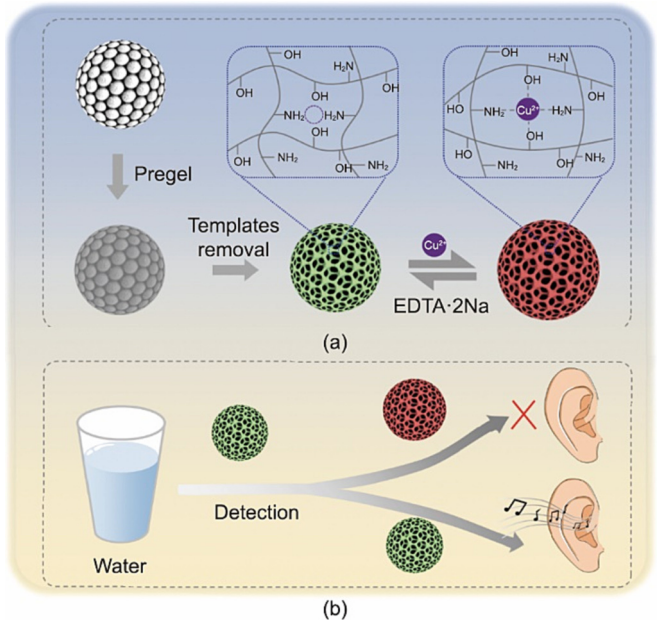

Fig. 1. Schematic diagrams of the fabrication process. (a) Response mechanism. (b) Application of the IIHBs. EDTA·2Na: ethylenediamine tetraacetic acid disodium.

with various cationic ions. Thus, it is widely used in many fields [28–36]. CS-based materials have been developed for the binding and removal of heavy metal ions [37–39]. However, their poor selectivity makes them unsuitable for the detection of heavy metal ions. By contrast, imprinted polymers are materials with imprinted sites that can specifically bind to imprinted molecules and ions specifically [40–42]. Therefore, ionically imprinted polymers (IIPs) are widely used for ion recognition and removal [43,44]. Inverse opals, a type of material with an ordered microporous structure that is generally fabricated by replicating colloidal crystals [45–53], have shown great potential in sensing, catalysis, and tissue engineering [54–61]. Owing to their unique microstructures, inverse opals exhibit vivid structural colors. In particular, when coupled with responsive hydrogels, the response of the hydrogels to the stimuli may cause a color change, which allows inverse opal hydrogels to be ideal sensors for the label-free detection of target stimuli.

We integrated a CS-based ionic imprinted hydrogel with structural color beads derived from the silica colloidal crystal beads (SCCBs) template to present a label-free detection platform for Cu^{2+}. A mixture of CS, polyethylene glycol diacrylate (PEGDA), and Cu^{2+} was used as a pregel to replicate the SCCBs. After polymerization of the pregel and removal of the Cu^{2+} and SCCB templates, IIHBs with inverse opal structures were obtained. The IIHBs exhibited a good degree of sphericity and monodispersity, and were coupled with magnetic nanoparticles to obtain mobility. When the IIHBs were immersed in a solution containing Cu^{2+}, they could recognize and rebind with the ions with high specificity and satisfactory repeatability and showed a shift in the reflective peak related to the concentration. Notably, we demonstrated that excess Cu^{2+} negatively influenced House Ear Institute-Organ of Corti 1 (HEI-OC1) cells' activity, revealing the positive significance of Cu^{2+} detection in hearing loss prevention. Subsequently, an assay of Cu^{2+} in tap water by spiking confirmed its potential for practical applications. These results suggest that the presented IIHBs are feasible as a facile, low-cost, and high-specificity detection platform for Cu^{2+}; therefore, they are promising indicators for foods and drinking water and prevent hearing loss.

2. Experimental section

2.1. Materials

CS (deacetylation degree 80%–95%, 50–800 mPa·s), ethylenediamine tetraacetic acid disodium (EDTA·2Na), $Cu(NO_3)_2$, $NaNO_3$, KNO_3, $Pb(NO_3)_2$, $Mg(NO_3)_2$, $Zn(NO_3)_2$, $Ca(NO_3)_2$, and $Al(NO_3)_3$ were bought from Shanghai Sinopharm Co., Ltd. (China). 2-hydroxy-2-methylpropiophenone photoinitiator (HMPP) and PEGDA were obtained from Sigma-Aldrich (USA). Glutaraldehyde (GA), hydrofluoric acid (HF; 40%, v/v), silicone oil, sodium diethyldithiocarbamate (DDTC·Na), and acetic acid were obtained from Macklin (China). All reagents were of analytical grade or higher and used as received. Water was purified and with a resistivity higher than 18 MΩ·cm.

2.2. Preparation of SCCBs

SCCBs were prepared according to a previously reported method. First, silica nanoparticles were dispersed in water to form homogeneous solutions (20%, w/v). The solution was then pumped into a single-emulsion microfluidic chip and cut into droplets using silicone oil. The droplets were collected in a container containing silicon oil and placed in an oven at 75 °C overnight. Subsequently, *n*-hexane was used to remove the silicon oil. Finally, the beads were collected in a crucible and calcined in a muffle furnace at 800 °C for 4 h.

2.3. Fabrication of CS-based IIHBs

A solution of CS (2%, w/v), $Cu(NO_3)_2$, and PEGDA (15%, w/v), was used as the pregel (20 μL) to infiltrate the SCCBs (number: approximately 200) for 6 h. The system was then polymerized under ultraviolet (UV) light for 10 s and treated with GA for 4 h. Thereafter, the beads were separated from the bulk hydrogel and incubated with EDTA·2Na solution (2%, w/v) for 3 h at a shaker. Finally, the beads were treated with HF (2%, w/v) for 2 h. The NIHBs were fabricated using the same process but without $Cu(NO_3)_2$.

2.4. Detection of Cu^{2+} using IIHBs

The reflection wavelengths of the IIHBs and NIHBs were measured before detection. They were then immersed in 3 mL of $Cu(NO_3)_2$ solution (0, 1, 10, 10^2, 10^3, 10^4, 10^5, and 10^6 nmol·L^{-1}) for 2 h. Finally, the IIHBs and NIHBs were washed gently, and their reflective wavelengths were measured again. The concentrations of IIHBs and NIHBs used in each group were 5.

2.5. Selectivity of IIHBs

The reflection wavelengths of the IIHBs were measured before detection. They were then incubated in a 3 mL solution containing different types of ions (10^5 nmol·L^{-1}) for 2 h. Finally, the IIHBs were washed gently and the reflective wavelength was measured again. The IIHBs used in each concentration groups were 5.

2.6. Quantitative analysis of IIHBs

The standard curve of Cu^{2+} was obtained by mixing the DDTC·Na solution with $Cu(NO_3)_2$ solutions at different concentrations for 10 min, and the absorbance of the solution at 452 nm was detected first. Thereafter, 300 μL IIHBs or NIHBs were incubated in 5 mL $Cu(NO_3)_2$ solution (200 μmol·L^{-1}) for 3 h, respectively. Subsequently, 50 μL of the supernatant was added to the mixture of 50 μL DDTC·Na solution (400 μmol·L^{-1}) and 100 μL

ammonia solution (pH 9.0–9.2) for 10 min. The absorbance of the solution was measured at 452 nm. Each experiment was repeated five times.

2.7. Cytotoxicity of Cu^{2+} on HEI-OC1 cells

HEI-OC1 cells were co-cultured with the culture medium containing 0, 20, 50, 100, 200, and 300 μmol·L^{-1} Cu^{2+} in a 12-well plate with glass coverslips. After incubation for 1 and 6 h, the cells were strained by adding 1 μL·mL^{-1} Calcein-AM and propidium iodide (PI) into the culture medium and incubated for 30 min at 37 °C. HEI-OC1 cells were added to 96-well plates and cultured in a medium containing 0, 20, 50, 100, 200, and 300 μmol·L^{-1} Cu^{2+}. After incubation for 1 and 6 h, the cells were treated with the cell counting kit-8 (CCK-8) in accordance with the manufacturer's instructions, and the absorbance was read using a microplate reader at 450 nm.

2.8. Detection of Cu^{2+} in tap water

The Cu^{2+} concentration in tap water was determined using the spiking method. The reflection wavelengths of the IIHBs were measured before detection. Thereafter, they were incubated in a 3 mL solution with different concentrations of Cu^{2+} (1, 5, 10, 50, and 100 μmol·L^{-1}, respectively) for 2 h. Finally, the IIHBs were washed gently and the reflective wavelength was measured again. The IIHBs used in each concentration group were 5.

3. Results and discussion

In a typical experiment, template SCCBs were prepared by microfluidics [62–69], which is a reliable technology that can generate microparticles and fibers with uniform size [70–72]. In brief, silica nanoparticles were dispersed in water to form a colloidal solution and used as the inner phase of a single-emulsion microfluidic chip, whereas silicon oil was employed as the outer phase. When the microfluidic system was operated, the inner phase was cut into droplets and collected in a container with silicone oil. After drying and calcination, the nanoparticles self-assembled into the SCCBs. Owing to the precise control of the microfluidics, the SCCBs exhibited good monodispersity (Fig. S1 in Appendix A). To obtain the IIHBs, a pregel solution containing CS, Cu^{2+} and PEGDA was used to replicate the microstructure of the SCCBs. It has been demonstrated that CS can bind with Cu^{2+} to form a complex structure through coordination bonds and electrostatic interactions, and then crosslink with glutaraldehyde to form a CS hydrogel. However, pure CS hydrogels often suffer from fragility and poor elasticity, as well as sightless color of the resultant IIHBs. Therefore, PEGDA was added to the pregel solution, which formed a soft hydrogel network after polymerization and improved the optical properties of the resulting hydrogel beads. When the SCCBs were incubated in the pregel solution, their nanovoids were filled with the solution, and silica/hydrogel composite beads were obtained after polymerization. Following treatment with EDTA·2Na and HF, the Cu^{2+} and silica templates were removed to acquire IIHBs [73,74].

The microstructures of the beads were through scanning electron microscopy (SEM), as shown in Fig. 2. It could be found that the silica nanoparticles assembled into the close-packed arrangement on the surface of an SCCB (Fig. 2(a)), and it extended to the inside (Fig. 2(b)). The packing of the nanoparticles formed many nanovoids within the SCCB, which the hydrogel filled to form silica/hydrogel composite beads (Fig. S2(a) in Appendix A). After removing the templates, the hydrogel-based IIHBs were obtained. However, the poor mechanical strength of the hydrogel often leads to the collapse of the microstructure (Fig. S2(b) in Appendix A). Thus, we used a high-crosslinking agent to form an inverse opal structure. As shown in Figs. 2(c) and (d), the beads displayed an ordered microporous structure on the surface and inside, indicating successful replication and inheritance of the microstructure of the SCCB.

The unique microstructure of the beads results in a photonic bandgap that inhibits the spread of light at a specific frequency and reflects it to exhibit the corresponding structural colors. In general, the peak position λ of the reflective wavelength can be estimated using the Bragg–Snell law:

$$\lambda = 1.633 d n_{\text{average}} \quad (1)$$

where d refers to the nearest center-to-center distance of the nanoparticles or nanopores, and n_{average} refers to the average refractive index of the entire bead. Therefore, by changing d and n_{average},

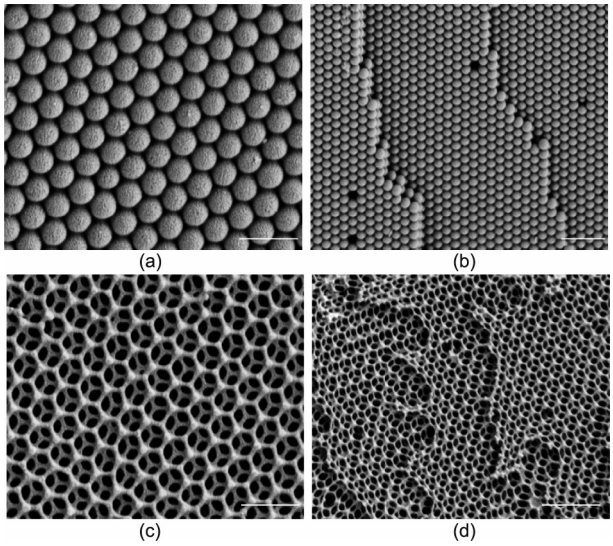

Fig. 2. SEM characterization. The (a) surface and (b) inside of an SCCB. The (c) surface and (d) inside of the inverse opal structure. Scale bars are 500 nm in (a) and (c), and 1 μm in (b) and (d).

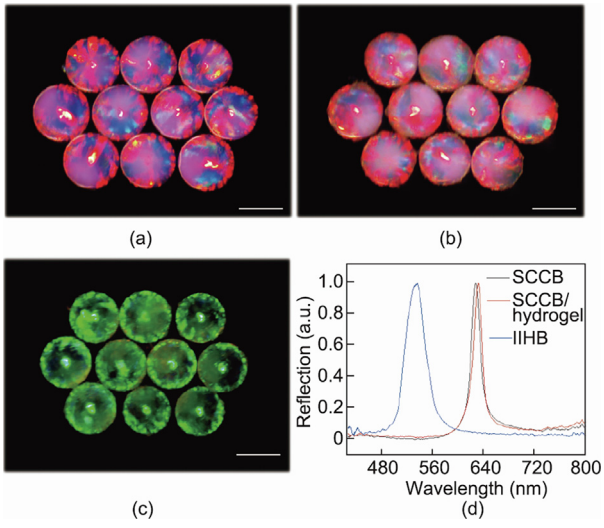

Fig. 3. Optical characterization. The optical images of (a) SCCBs with red color, (b) the corresponding composited beads, and (c) IIHBs. (d) The corresponding reflective wavelength of the beads in (a–c). Scale bars are 200 μm in (a–c). a.u.: arbitrary units.

the structural color of the beads can be tuned. In this study, the components of the beads and the ambient solution environment exhibited negligible changes; thus, $n_{average}$ was relatively stable, and the structural color was mainly dependent on d. As shown in Fig. 3(a) and Figs. S3 and S4 in Appendix A, silica nanoparticles of different sizes formed SCCBs with different structural colors. Moreover, the composite beads and IIHBs derived from the SCCBs displayed colors corresponding to those of the SCCBs (Figs. 3(b) and (c)). Generally, the composite beads had the same d as the SCCBs but a slightly higher $n_{average}$, which led to a slight red shift of the color. In contrast, IIHBs had a lower $n_{average}$ and thus displayed an apparent blue shift (Fig. 3; Figs. S3 and S4).

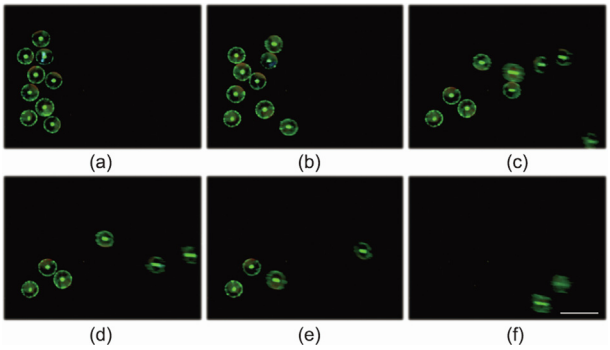

Fig. 4. Magnetic field-regulated movability. (a) The IIHBs at the initial position. (b–f) The movement of the IIHBs under the trigger of the magnetic field. Scale bar is 500 μm.

Notably, the IIHBs had a similar density to that of water. Therefore, to realize fast separation of IIHBs from the solution, IIHBs were functionalized with magnetic nanoparticles to obtain magnetic field-regulated mobility. As shown in Fig. 4 and Movie S1 in Appendix A, the functionalized IIHBs were initially placed on one side of a dish. When a magnetic field was applied to the other side, the IIHBs displayed excellent responsiveness and moved quickly in the direction of the magnetic field. This result indicates that the IIHBs could be easily enriched and separated from the solution using a magnet, which made it possible to save time in collecting the IIHBs.

When IIHBs were incubated in a solution containing Cu^{2+}, they bound to the ions and showed changes in the reflective wavelength peak. As shown in Fig. 5, the IIHBs displayed a red shift in the Cu^{2+} solution, and the shift increased with the concentration of Cu^{2+}. In addition, the shift values of the IIHBs were significantly different from those of non-imprinted hydrogel beads (NIHBs), indicating that the shift was caused by the interaction between the imprinted sites and Cu^{2+}. Therefore, by simply measuring the reflective wavelength of the IIHBs before and after incubation in the solution, the

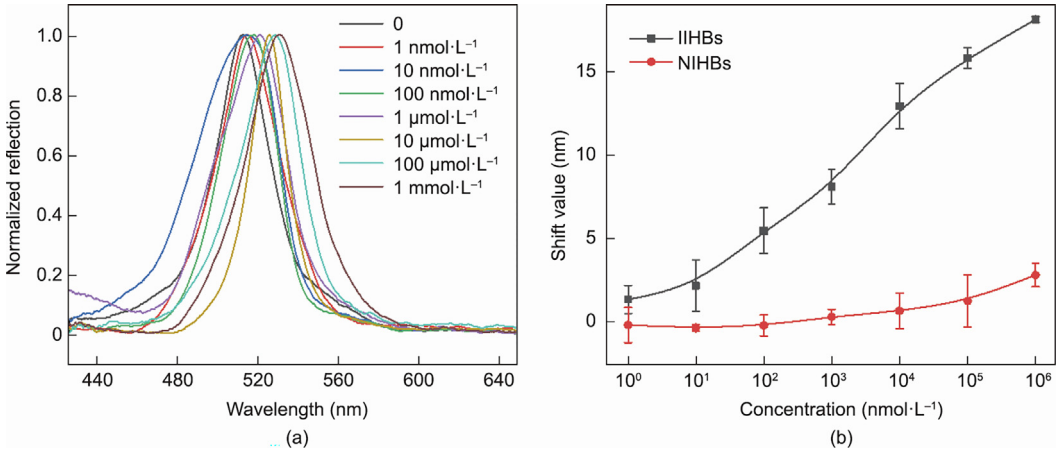

Fig. 5. Cu^{2+} detection capability of IIHBs. (a) The reflective wavelength of the IIHBs incubated in different concentrations of Cu^{2+}. (b) The shift value of the IIHBs and NIHBs in the different concentrations of Cu^{2+}.

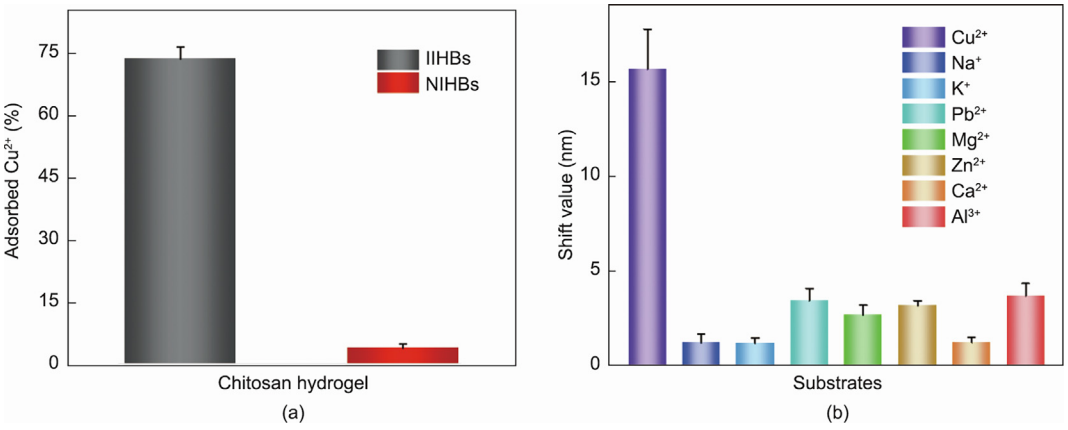

Fig. 6. Specificity and selectivity of the IIHBs. (a) Comparison of the Cu^{2+} adsorption capability of IIHBs and NIHBs. (b) The shift value of the IIHBs in the solution containing different types of ions. The concentrations in all the groups were 100 μmol·L^{-1}.

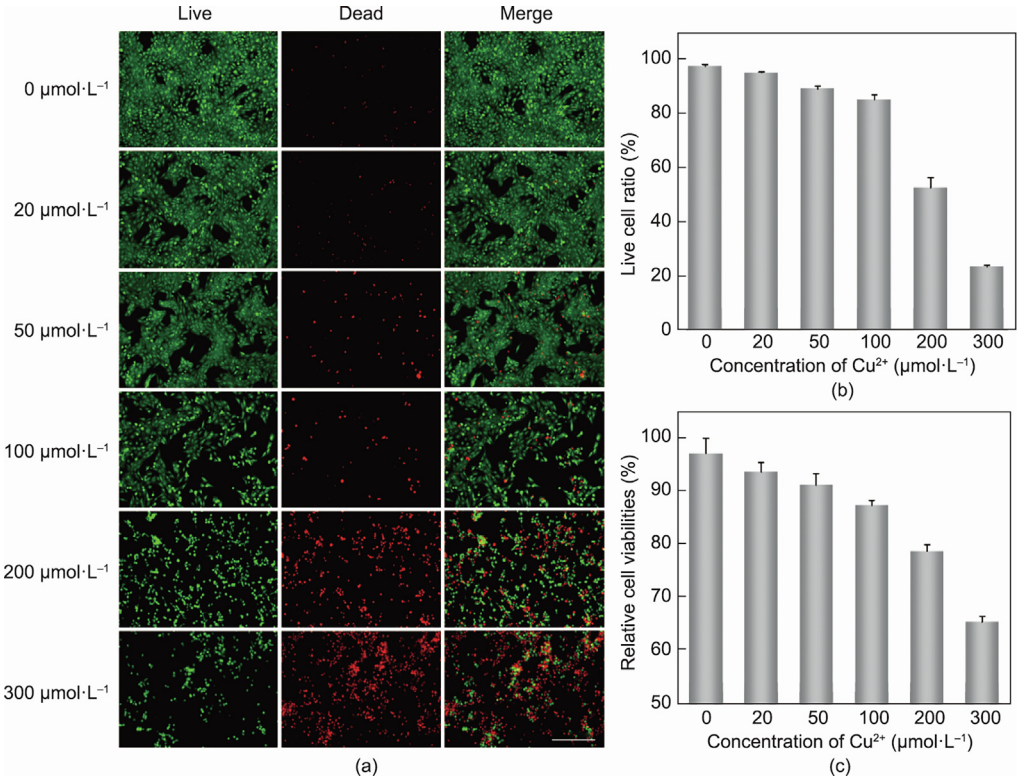

Fig. 7. Cytotoxicity of Cu^{2+} on HEI-OC1 cells. (a) Live/dead staining results of HEI-OC1 cells in medium with different concentrations of Cu^{2+} after 6 h culture. (b) Live/dead ratio and (c) cell viabilities of HEI-OC1 cells in medium with different concentrations of Cu^{2+} after 6 h culture. Scale bar is 500 μm.

assay of Cu^{2+} concentration could be realized without any labels. Notably, although a higher concentration of Cu^{2+} resulted in a larger shift value of the IIHBs, the shift value of the NIHBs also increased in this case, indicating that more non-specific adsorption occurred. To ensure detection accuracy, IIHBs should be used in solutions containing Cu^{2+} at concentrations lower than 1 mmol·L^{-1}

The different binding capabilities of IIHBs and NIHBs to Cu^{2+} were further studied by quantitative analysis. DDTC·Na is a sensitive reagent for Cu detection. It can form a brown–yellow complex with Cu^{2+} in the ammonia solution with pH 9.0–9.2, and the complex has an apparent peak of absorbance at 452 nm (Fig. S5(a) in Appendix A). The absorbance exhibited a linear relationship with the concentration of Cu^{2+} (Fig. S5(b) in Appendix A). Based on this mechanism, we incubated IIHBs and NIHBs in the Cu^{2+} solution (100 μmol·L^{-1}) for 3 h and analyzed the residual concentration of Cu^{2+} after the reaction. As shown in Fig. 6(a) and Table S1 in Appendix A, the IIHBs and NIHBs displayed a wide difference in Cu^{2+} adsorption, with an imprinting factor (IF) of 19.14, indicating the good specificity of the developed IIHBs.

In addition, the selectivity of the IIHBs was studied. For this purpose, the IIHBs were treated 100 μmol·L^{-1} solution with different cations. The IIHBs showed a large shift value (15.67 nm) in the Cu^{2+} solution, whereas the value in the solution of other types of ions was smaller than 4 nm, confirming the accurate selectivity of the IIHBs for Cu^{2+} detection (Fig. 6(b)).

According to previous studies, excess Cu^{2+} generates hydroxyl radicals and induce HC apoptosis to lead to hearing loss. Therefore, it is important to monitor Cu^{2+} levels in drinking water to control Cu^{2+} uptake. Before being applied in practical application, the influence of Cu^{2+} on HEI-OC1 cells was studied. As shown in Figs. 7(a) and (b), HEI-OC1 cells displayed normal growth in the culture medium without Cu^{2+}. However, when Cu^{2+} was added to the medium, cell viability reduced, and this reduction was closely related to the concentration of added Cu^{2+}. The results of the cell viability assay agreed with those of the live/dead staining (Fig. 7(c)). These results confirmed that Cu^{2+} severely damaged HEI-OC1 cells, indicating that it is necessary to avoid high Cu^{2+} intake to prevent hearing loss. To achieve this goal, we used the developed IIHBs to monitor Cu^{2+} in food and drinking water. For example, they have been used to assay Cu^{2+} in tap water using a spiking strategy. As shown in Table 1 and Fig. S6 in Appendix A, the IIHBs in the solution displayed a shift in value with the added amount, and the recoveries were acceptable when compared with the standard curve, revealing little Cu^{2+} in the tap water. These results indicated that the prepared IIHBs are promising for the Cu^{2+} detection of actual samples.

Table 1
Determination of Cu^{2+} in spiked tap water by IIHBs.

Spiked (μmol·L^{-1})	Detected (μmol·L^{-1})	Recovery (%)	RSD (%)
1	0.853	85	3.9
5	5.220	104	5.1
10	8.830	88	4.2
50	47.060	94	6.5
100	114.040	114	4.9

4. Conclusion

In summary, we developed novel CS-based IIHBs with a spherical shape, uniform size, and magnetic responsiveness for the label-free detection of Cu^{2+} in water to prevent excessive Cu^{2+} uptake and hearing loss. The CS component could bind with Cu^{2+} to form imprinting sites, whereas PEGDA improved the mechanical properties of the hydrogels. When IIHBs were incubated in a solution containing ions, they could specifically bind to Cu^{2+} and showed a

redshift in the reflective wavelength peak, which could sense the concentration that could cause damage to HEI-OC1 cells. The applicability of IIHBs was also evaluated by spiking them with tap water. These features indicate that the developed IIHBs are feasible for detecting Cu^{2+} in water and are promising indicators for food and drinking water to prevent hearing loss.

Acknowledgments

This work was supported by grants from the National Key Research and Development Program of China (2021YFA1101300, 2021YFA1101800, and 2020YFA0112503); the National Natural Science Foundation of China (82030029, 81970882, 92149304, and 22302231); the Science and Technology Department of Sichuan Province (2021YFS0371); the Guangdong Basic and Applied Basic Research Foundation (2023A1515011986); the Shenzhen Fundamental Research Program (JCYJ20190814093401920, JCYJ20210324125608022, JCYJ20190813152616459, and JCYJ20190808120405672); the Futian Healthcare Research Project (FTWS2022013 and FTWS2023080); the Open Research Fund of State Key Laboratory of Genetic Engineering, Fudan University (SKLGE-2104); and the Fundamental Research Funds for the Central Universities, Sun Yat-sen University (23qnpy153).

Authors' contribution

Huan Wang and Renjie Chai provided the idea and designed the experiment. Huan Wang carried out experiments and data analysis. Huan Wang and Hui Zhang wrote the manuscript. Xiaoli Zhang, Hong Chen, and Ling Lu contributed to the scientific discussion.

Compliance with ethics guidelines

Huan Wang, Hui Zhang, Xiaoli Zhang, Hong Chen, Ling Lu, and Renjie Chai declare that they have no conflict of interest or financial conflicts to disclose.

Appendix A. Supplementary data

Supplementary data to this article can be found online at https://doi.org/10.1016/j.eng.2023.09.001.

References

[1] Haile LM, Kamenov K, Briant PS, Orji AU, Steinmetz JD, Abdoli A, et al. Hearing loss prevalence and years lived with disability, 1990–2019: findings from the Global Burden of Disease Study 2019. Lancet 2021;397(10278):996–1009.
[2] Li CM, Zhang X, Hoffman HJ, Cotch MF, Themann CL, Wilson MR. Hearing impairment associated with depression in US adults, National Health and Nutrition Examination Survey 2005–2010. Jama Otolaryngol 2014;140(4):293–302.
[3] Chadha S, Kamenov K, Cieza A. The world report on hearing, 2021. Bull WHO 2021;99(4). 242–A.
[4] Chen H, Zhang H, Dai Y, Zhu H, Hong G, Zhu C, et al. Magnetic hydrogel microrobots delivery system for deafness prevention. Adv Funct Mater 2023;33(35):2303011.
[5] Monzani D, Galeazzi GM, Genovese E, Marrara A, Martini A. Psychological profile and social behaviour of working adults with mild or moderate hearing loss. Acta Otorhinolaryngol 2008;28(2):61–6.
[6] Abdelrahman EA, Abou El-Reash YG, Youssef HM, Kotp YH, Hegazey RM. Utilization of rice husk and waste aluminum cans for the synthesis of some nanosized zeolite, zeolite/zeolite, and geopolymer/zeolite products for the efficient removal of Co(II), Cu(II), and Zn(II) ions from aqueous media. J Hazard Mater 2021;401:123813.
[7] Fayazi M, Ghanei-Motlagh M, Karami C. Application of magnetic nanoparticles modified with *L*-cysteine for pre-concentration and voltammetric detection of copper(II). Microchem J 2022;181:107652.
[8] Ye K, Zhang G, Ni B, Guo L, Deng C, Zhuang X, et al. Steering CO_2 electrolysis selectivity by modulating the local reaction environment: an online DEMS approach for Cu electrodes. eScience 2023;3(4):100143.
[9] Bai S, Qiu H, Song M, He G, Wang F, Liu Y, et al. Porous fixed-bed photoreactor for boosting C–C coupling in photocatalytic CO_2 reduction. eScience 2022;2(4):428–37.
[10] Xiong F, Jiang Y, Cheng L, Yu R, Tan S, Tang C, et al. Low-strain TiP_2O_7 with three-dimensional ion channels as long-life and high-rate anode material for Mg-ion batteries. Interdiscip Mater 2022;1(1):140–7.
[11] Tang S, Lin L, Wang X, Yu A, Sun X. Interfacial interactions between collected nylon microplastics and three divalent metal ions (Cu(II), Ni(II), Zn(II)) in aqueous solutions. J Hazard Mater 2021;403:123548.
[12] Yang W, Li J, Lyu Y, Yan X, Yang P, Zuo M. Bioinspired 3D hierarchical BSA-$NiCo_2O_4$@MnO_2/C multifunctional micromotors for simultaneous spectrophotometric determination of enzyme activity and pollutant removal. J Clean Prod 2021;309:127294.
[13] Xiao T, Wang Y, Hao Y, Cai Z, Song M, He J, et al. Resonance Rayleigh scattering method for highly sensitive detection of copper ions in water based on salicylaldeoxime-copper (II)-2-methylimidazole supramolecular. Microchem J 2022;181:107744.
[14] Ou P, Tritschler HJ, Wolff SP. Thioctic (lipoic) acid: a therapeutic metal-chelating antioxidant? Biochem Pharmacol 1995;50(1):123–6.
[15] Yu H, Lin Q, Wang Y, He Y, Fu S, Jiang H, et al. Inhibition of H3K9 methyltransferases G9a/GLP prevents ototoxicity and ongoing hair cell death. Cell Death Dis 2013;4(2):e506.
[16] Monroe JD, Rajadinakaran G, Smith ME. Sensory hair cell death and regeneration in fishes. Front Cell Neurosci 2015;9:131.
[17] Olivari FA, Hernandez PP, Allende ML. Acute copper exposure induces oxidative stress and cell death in lateral line hair cells of zebrafish larvae. Brain Res 2008;1244:1–12.
[18] Hernandez PP, Moreno V, Olivari FA, Allende ML. Sub-lethal concentrations of waterborne copper are toxic to lateral line neuromasts in zebrafish (*Danio rerio*). Hear Res 2006;213(1–2):1–10.
[19] Wu X, Meng X, Hou B, Sun Z, Zhang Y, Li M. Rapid fluorescent color analysis of copper ions on a smart phone via ratiometric fluorescence sensor. Microchim Acta 2022;189(2):67.
[20] Okamoto Y, Kishikawa N, Hagimori M, El-Maghrabey M, Kawakami S, Kuroda N. A turn-on hydrazide oxidative decomposition-based fluorescence probe for highly selective detection of Cu^{2+} in tap water as well as cell imaging. Anal Chim Acta 2022;1217:340024.
[21] Ho VTTX, Park H, An S, Kim G, Ly NH, Lee SY, et al. Coumarin–lipoic acid conjugates on silver nanoparticle-supported nanopipettes for *in situ* dual-mode monitoring of intracellular Cu(II) and potential chemodynamic therapy applications. Sens Actuators B 2021;344:130271.
[22] Lutfullah S, Sharma S, Rahman N, Azmi SNH, Iqbal B, Amburk MIBB, et al. UV spectrophotometric determination of Cu(II) in synthetic mixture and water samples. J Chin Chem Soc 2010;57(4A):622–31.
[23] Manousi N, Kabir A, Furton KG, Anthemidis AN. Dual lab-in-syringe flow-batch platform for automatic fabric disk sorptive extraction/back-extraction as a front end to inductively coupled plasma atomic emission spectrometry. Anal Chem 2022;94(38):12943–7.
[24] Larner F, Rehkämper M, Coles BJ, Kreissig K, Weiss DJ, Sampson B, et al. A new separation procedure for Cu prior to stable isotope analysis by MC-ICP-MS. J Anal At Spectrom 2011;26(8):1627–32.
[25] González-Álvarez RJ, Bellido-Milla D, Pinto JJ, Moreno C. A handling-free methodology for rapid determination of Cu species in seawater based on direct solid micro-samplers analysis by high-resolution continuum source graphite furnace atomic absorption spectrometry. Talanta 2020;206:120249.
[26] El Badry MM, Frag EY, El Brawy MH. Rapid potentiometric sensor for determination of Cu(II) ions in food samples. Microchem J 2021;164:106065.
[27] Liu T, Zhou M, Pu Y, Liu L, Li F, Li M, et al. Silver nanoparticle-functionalized 3D flower-like copper (II)-porphyrin framework nanocomposites as signal enhancers for fabricating a sensitive glutathione electrochemical sensor. Sens Actuators B 2021;342:130047.
[28] Wang H, Zhang H, Xie Z, Chen K, Ma M, Huang Y, et al. Injectable hydrogels for spinal cord injury repair. Eng Regen 2022;3(4):407–19.
[29] Ma Y, Chen Q, Li W, Su H, Li S, Zhu Y, et al. Spinal cord conduits for spinal cord injury regeneration. Eng Regen 2023;4(1):68–80.
[30] Qiu L, Kong B, Kong T, Wang H. Recent advances in liver-on-chips: design, fabrication, and applications. Smart Med 2023;2(1):20220010.
[31] Zhang H, Xu D, Zhang Y, Li M, Chai R. Silk fibroin hydrogels for biomedical applications. Smart Med 2022;1(1):e20220011.
[32] Liu S, Yu JM, Gan YC, Qiu XZ, Gao ZC, Wang H, et al. Biomimetic natural biomaterials for tissue engineering and regenerative medicine: new biosynthesis methods, recent advances, and emerging applications. Mil Med Res 2023;10(1):16.
[33] Wang J, Huang D, Yu H, Cheng Y, Ren H, Zhao Y. Developing tissue engineering strategies for liver regeneration. Eng Regen 2022;3(1):80–91.
[34] Furtado M, Chen L, Chen Z, Chen A, Cui W. Development of fish collagen in tissue regeneration and drug delivery. Eng Regen 2022;3(3):217–31.
[35] Li D, Yue G, Li S, Liu J, Li H, Gao Y, et al. Fabrication and applications of multi-fluidic electrospinning multi-structure hollow and core–shell nanofibers. Engineering 2022;13:116–27.
[36] Zhou L, Guo P, D'Este M, Tong W, Xu J, Yao H, et al. Functionalized hydrogels for articular cartilage tissue engineering. Engineering 2022;13:71–90.
[37] Peighambardoust SJ, Aghamohammadi-Bavil O, Foroutan R, Arsalani N. Removal of malachite green using carboxymethyl cellulose-g-polyacrylamide/montmorillonite nanocomposite hydrogel. Int J Biol Macromol 2020;159:1122–31.

[38] Hajri AK, Jamoussi B, Albalawi AE, Alhawiti OHN, Alsharif AA. Designing of modified ion-imprinted chitosan particles for selective removal of mercury (II) ions. Carbohydr Polym 2022;286:119207.
[39] Upadhyay U, Sreedhar I, Singh SA, Patel CM, Anitha KL. Recent advances in heavy metal removal by chitosan based adsorbents. Carbohydr Polym 2021;251:117000.
[40] Guo Z, Zhao M, Liu Z. Molecularly imprinted and cladded nanoparticles for high-affinity recognition of structurally closed gangliosides. Microchim Acta 2022;189(8):289.
[41] Pang J, Li P, He H, Xu S, Liu Z. Molecularly imprinted polymers outperform lectin counterparts and enable more precise cancer diagnosis. Chem Sci 2022;13(16):4589–97.
[42] Xing R, Guo Z, Lu H, Zhang Q, Liu Z. Molecular imprinting and cladding produces antibody mimics with significantly improved affinity and specificity. Sci Bull 2022;67(3):278–87.
[43] Alizadeh T, Mousavi Z. Molecularly imprinted polymer specific to creatinine complex with copper(II) ions for voltammetric determination of creatinine. Microchim Acta 2022;189(10):393.
[44] Wang X, Chu Z, Huang Y, Chen G, Zhao X, Zhu Z, et al. Copper ion imprinted hydrogel photonic crystal sensor film. ACS Appl Polym Mater 2022;4(6):4568–75.
[45] Wang H, Liu Y, Chen Z, Sun L, Zhao Y. Anisotropic structural color particles from colloidal phase separation. Sci Adv 2020;6(2):eaay1438.
[46] Wei X, Bian F, Zhang H, Wang H, Zhu Y. Multiplex assays of bladder cancer protein markers with magnetic structural color hydrogel microcarriers based on microfluidics. Sens Actuators B 2021;346:130464.
[47] Zhang H, Zhang Z, Zhang H, Chen C, Zhang D, Zhao Y. Protein-based hybrid responsive microparticles for wound healing. ACS Appl Mater Interfaces 2021;13(16):18413–22.
[48] Zhang H, Guo J, Wang Y, Sun L, Zhao Y. Stretchable and conductive composite structural color hydrogel films as bionic electronic skins. Adv Sci 2021;8(20):2102156.
[49] Zhang H, Liu Y, Chen G, Wang H, Chen C, Li M, et al. Immunotherapeutic silk inverse opal particles for post-surgical tumor treatment. Sci Bull 2020;65(5):380–8.
[50] Wang H, Zhao Z, Liu YX, Shao CM, Bian FK, Zhao YJ. Biomimetic enzyme cascade reaction system in microfluidic electrospray microcapsules. Sci Adv 2018;4(6):eaat2816.
[51] Zhang Z, Chen Z, Wang Y, Chi J, Wang Y, Zhao Y. Bioinspired bilayer structural color hydrogel actuator with multienvironment responsiveness and survivability. Small Methods 2019;3(12):1900519.
[52] Sun L, Chen Z, Bian F, Zhao Y. Bioinspired soft robotic caterpillar with cardiomyocyte drivers. Adv Funct Mater 2020;30(6):1907820.
[53] Zhang H, Wang H, Wen B, Lu L, Zhao Y, Chai R. Ultrasound-responsive composited conductive silk conduits for peripheral nerve regeneration. Small Struct 2023;4(9):2300045.
[54] Zhang H, Guo J, Wang Y, Shang L, Chai R, Zhao Y. Natural polymer-derived bioscaffolds for peripheral nerve regeneration. Adv Funct Mater 2022;32(41):2203829.
[55] Wang H, Gu H, Chen Z, Shang L, Zhao Z, Gu Z, et al. Enzymatic inverse opal hydrogel particles for biocatalyst. ACS Appl Mater Interfaces 2017;9(15):12914–8.
[56] Wang H, Cai L, Zhang D, Shang L, Zhao Y. Responsive janus structural color hydrogel micromotors for label-free multiplex assays. Research 2021;2021:9829068.
[57] Wang H, Zhang H, Zhang D, Wang J, Tan H, Kong T. Enzyme-functionalized structural color hydrogel particles for urea detection and elimination. J Clean Prod 2021;315:128149.
[58] Wang H, Wang J, Wang Y, Liu Y, Liu R, Wang X, et al. Oriented boronate affinity-imprinted inverse opal hydrogel for glycoprotein assay via colorimetry. Microchim Acta 2020;187(6):348.
[59] Hu Y, Zhang H, Wei H, Liao M, Chen X, Xing J, et al. Conductive PS inverse opals for regulating proliferation and differentiation of neural stem cells. Eng Regen 2023;4(2):214–21.
[60] Zhang H, Zhang H, Wang H, Zhao Y, Chai R. Natural proteins-derived asymmetric porous conduit for peripheral nerve regeneration. Appl Mater Today 2022;27:101431.
[61] Fu F, Chen Z, Wang H, Liu C, Liu Y, Zhao Y. Graphene hybrid colloidal crystal arrays with photo-controllable structural colors. Nanoscale 2019;11(22):10846–51.
[62] Shang L, Cheng Y, Zhao Y. Emerging droplet microfluidics. Chem Rev 2017;117(12):7964–8040.
[63] Shang L, Ye F, Li M, Zhao Y. Spatial confinement toward creating artificial living systems. Chem Soc Rev 2022;51(10):4075–93.
[64] Wang J, Huang D, Ren H, Shang L. Biomimic trained immunity-MSCs delivery microcarriers for acute liver failure regeneration. Small 2022;18(36):2200858.
[65] Zhang H, Liu Y, Chen C, Cui W, Zhang C, Ye F, et al. Responsive drug-delivery microcarriers based on the silk fibroin inverse opal scaffolds for controllable drug release. Appl Mater Today 2020;19:100540.
[66] Hao Y, Hu F, Chen Y, Wang Y, Xue J, Yang S, et al. Recent progress of electrospun nanofibers for zinc–air batteries. Adv Fiber Mater 2021;4(2):185–202.
[67] Hu J, Zhao XW, Zhao YJ, Li J, Xu WY, Wen ZY, et al. Photonic crystal hydrogel beads used for multiplex biomolecular detection. J Mater Chem 2009;19:5730–6.
[68] Zhao Y, Zhao X, Pei X, Hu J, Zhao W, Chen B, et al. Multiplex detection of tumor markers with photonic suspension array. Anal Chim Acta 2009;633(1):103–8.
[69] Luo Z, Che J, Sun L, Yang L, Zu Y, Wang H, et al. Microfluidic electrospray photo-crosslinkable κ-Carrageenan microparticles for wound healing. Eng Regen 2021;2:257–62.
[70] Wang H, Zhang H, Chen Z, Zhao Y, Gu Z, Shang L. Polymer-based responsive structural color materials. Prog Mater Sci 2023;135:101091.
[71] Zhu Y, Kong B, Liu R, Zhao Y. Developing biomedical engineering technologies for reproductive medicine. Smart Med 2022;1(1):e20220006.
[72] Gao Y, Ma Q. Bacterial infection microenvironment-responsive porous microspheres by microfluidics for promoting anti-infective therapy. Smart Med 2022;1(1):e20220012.
[73] Monier M, Bukhari AAH, Elsayed NH. Designing and characterization of copper (II) ion-imprinted adsorbent based on isatin functionalized chitosan. Int J Biol Macromol 2020;155:795–804.
[74] Shao C, Yu Y, Fan Q, Wang X, Ye F. Polyurethane-polypyrrole hybrid structural color films for dual-signal mechanics sensing. Smart Med 2022;1(1):e20220008.